# Subtract the Corruption: Training-Data-Free Corrective Machine Unlearning using Task Arithmetic

# Mostafa Mozafari Farooq Ahmad Wani Maria Sofia Bucarelli Fabrizio Silvestri Sapienza University of Rome

mostafamozafari1996@gmail.com, farooqahmad.wani@uniromal.it mariasofia.bucarelli@uniromal.it, fsilvestri@diag.uniromal.it

# **Abstract**

Corrupted training data are ubiquitous. Corrective Machine Unlearning (CMU) seeks to remove the influence of such corruption post-training. Prior CMU typically assumes access to identified corrupted training samples (a "forget set"). However, in many real-world scenarios the training data are no longer accessible. We formalize source-free CMU, where the original training data are unavailable and, consequently, no forget set of identified corrupted training samples can be specified. Instead, we assume a small proxy (surrogate) set of corrupted samples that reflect the suspected corruption type without needing to be the original training samples. In this stricter setting, methods relying on forget set are ineffective or narrow in scope. We introduce Corrective Unlearning in Task Space (CUTS), a lightweight weight space correction method guided by the proxy set using task arithmetic principles. CUTS treats the clean and the corruption signal as distinct tasks. Specifically, we briefly fine-tune the corrupted model on the proxy to amplify the corruption mechanism in the weight space, compute the difference between the corrupted and fine-tuned weights as a proxy task vector, and subtract a calibrated multiple of this vector to cancel the corruption. Without access to clean data or a forget set, CUTS recovers a large fraction of the lost utility under label noise and, for backdoor triggers, nearly eliminates the attack with minimal damage to utility, outperforming state-of-the-art specialized CMU methods in source-free setting. Code is available at https://github.com/mosix11/CUTS.

# 1. Introduction

Deep neural networks owe much of their success to training on massive and diverse datasets with human or automated annotations [69]. However, such datasets inevitably contain corrupted samples due to labeling mistakes, web-scale collection artifacts, or adversarial manipulations [2, 4, 5, 8, 10,

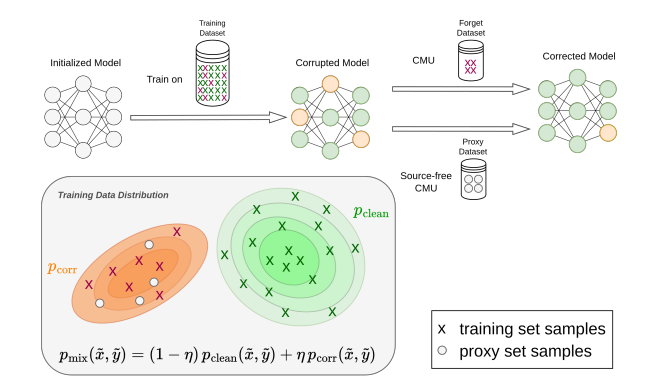


Figure 1. The training distribution mixes clean and corrupted distributions. Classic CMU corrects via an identified *forget set* of corrupted training samples. In source-free setting, the training dataset is inaccessible; one can only use a *proxy set* of samples from the corruption distribution not necessarily seen during training.

12, 19, 41, 56]. As dataset sizes grow, ensuring perfect data integrity becomes unrealistic, and modern overparameterized models tend to memorize or amplify the effects of these corruptions [1, 23, 49, 57]. A large body of work attempts to prevent corruption during data curation or training. For label noise, methods include *noise cleansing* [27, 32, 46, 59, 64] and *noise-robust learning* with robust losses [44, 62, 63, 73] or regularization [39, 66]. Similarly, for backdoor attacks, analogous up-front defenses include pre-training data sanitization as well as training procedures that are robust to triggered training samples [11, 29, 38, 48, 57, 60, 74]. Yet these approaches rely on access to the full training set and are inapplicable once the model has already been trained. In many real-world scenarios, the corruption is discovered only after training or deployment and retraining might be costly and time consuming. This motivates post-training Corrective Machine Unlearning (CMU) [23], which aims to remove the detrimental effects of corrupted data from a trained model with minimal data, computation, and downtime. Unlike Privacy-Preserving Unlearning ([6, 21, 26, 68]), CMU does not require per-sample deletion guarantees, and targets the broader harmful effects of corruption.

In real-world deployments the original training data are often inaccessible or too costly to reproduce due to privacy, licensing, or operational constraints. However, post-deployment monitoring, red-teaming, or incident reports can reveal patterns consistent with specific classes of corruption [23]. To address this, we introduce and formalize the source-free CMU setting, where only the trained model and an identified corruption type are available, without access to any original training data (Fig. 1). Then, a practitioner compiles a small proxy (surrogate) dataset drawn from the same input domain or a close approximation (e.g., collected unlabeled samples, inference data, or generated data) and instantiates the suspected corruption on this proxy, such as injecting label noise or trigger patterns. Critically, this setup imposes weaker requirements than the classic CMU paradigm, which requires access to the actual corrupted training samples, necessitating storage of original data and identification of (a subset of) exact corrupted instances.

Task Arithmetic [30] has been shown effective in model editing. Adding task vectors to a pre-trained model can approximate multi-task behavior, and negating them can induce partial forgetting of the tasks. Our key hypothesis is that training on partially corrupted data can be viewed as a two-task learning problem; a clean task and a corruption task. The total weight update is thus approximately the sum of two task vectors in weight space. If we can estimate the corruption task vector using a proxy dataset, we can subtract it from the trained weights to cancel the corruption effect (Fig. 2). This builds on the observed local linearity and additivity of task vectors in pre-trained models [31, 37, 50, 71]. Practically, we fine-tune the corrupted model on the proxy with simulated corruption, extract the weight difference as the corruption task vector, then apply a scaled negative edit. This lightweight, source-free procedure effectively mitigates the detrimental impact of symmetric/asymmetric label noise [40] and BadNets-style triggers [25].

#### Contributions.

- We formalize *source-free Corrective Machine Unlearn-ing*, where the goal is to correct corrupted models using only a small *proxy* dataset of corrupted samples, without access to the original training data and forget set.
- We propose a post-training corrective method (CUTS) based on *task arithmetic*, treating corruption itself as a task. By estimating a corruption task vector using the proxy dataset, we show that the effect of corruption in corrupted models is encoded along an approximately linear direction in weight space, largely but not entirely distinct from the clean signal.

We demonstrate that CUTS is effective across a spectrum of corruption regularity, from unstructured corruptions (e.g., random label noise, which induces per-sample memorization) to structured ones (e.g., backdoor triggers with consistent learnable patterns), by targeting and counteracting corruption approximated directions in weight space rather than per-sample associations.

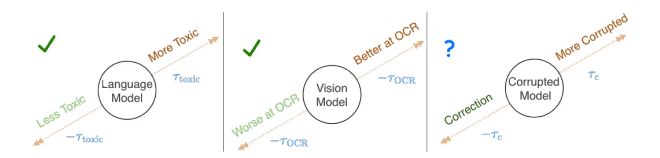


Figure 2. Task vector subtraction from a pre-trained model induces partial task forgetting, as demonstrated for partial unlearning of toxic language and degrading OCR performance in [30]. Our motivation is the following: if corruption can be modeled as a task, task arithmetic enables source-free, proxy-guided CMU.

We conduct extensive experiments across architectures (pre-trained and randomly initialized), datasets, and corruption types, providing a systematic analysis of our method's effectiveness, generalization, and limitations.

# 2. Related Works

Regularity and the Interplay Between Corruption and Memorization. Deep neural networks are known to memorize arbitrary data [1, 72]. This memorization supports learning from rare or atypical examples [16, 17]. Contrary to earlier assumptions [3, 58], memorization is not confined to specific layers but distributed across neurons throughout the network, and memorizing mislabeled and hard samples shows similar dynamics [45].

Regularity refers to the degree of self-similarity among corrupted examples [54]. Low-regularity corruptions (e.g., random label noise) lack structure and force the network to rely on per-sample memorization, while high-regularity corruptions (e.g., spatial backdoor triggers) provide consistent patterns that are easily learned and generalized. Consequently, memorization burden increases with decreasing regularity [45, 54]. This distinction underlines that memorization and corruption are intertwined, but their relationship depends critically on the regularity of the corruption.

Corrective Machine Unlearning. Machine unlearning seeks to remove the influence of specific training data from a model, ideally as if those samples had never been seen [7]. Early work motivated by privacy regulations proposed exact or approximate forgetting mechanisms [6, 21, 26], later expanded through influence-based updates [24] and distillation methods. Recent surveys [61, 68] classify approaches by efficiency and privacy fidelity. Beyond privacy, unlearning has become essential for removing corrupted or misla-

beled data discovered post-training. Goel et al. [23] formalized Corrective Machine Unlearning (CMU), which aims to mitigate the impact of corrupted samples while preserving model utility. Unlike classical unlearning that assumes all deletion data are known, CMU methods must operate under partial discovery and diverse corruption types. Studies show that existing methods perform inconsistently across corruption regularities, motivating methods that adaptively handle a wider range of corruptions [23, 54]. However, the majority of prior CMU approaches [13, 18, 23, 35, 54] require access to some identified corrupted samples from the original training data or the entire training data, making them impractical when data are unavailable due to legal or operational constraints. Our source-free formulation relaxes these assumptions. Among existing CMU methods, SAP [33] (for label noise) and Potion [53] (for poison triggers) are specialized SOTA approaches that can be adapted to source-free setting, and [22] provides a trivial catastrophic forgetting baseline via fine-tuning on a small clean set.

Task Arithmetic for Model Editing. Task arithmetic [30] offers a lightweight, data-free paradigm for model editing by operating on task vectors in the weight space. Model behaviors can be composed, removed, or transferred through linear combinations of task-specific vectors, enabling fast adaptation without joint fine-tuning. The success of task arithmetic has been linked to weight disentanglement; the property that different task directions act on largely disjoint functional regions, minimizing interference between edits [50]. Recent works have also begun to establish theoretical foundations for task arithmetic, explaining when and why it succeeds in nonlinear settings [31, 37, 71], although these analyses often rely on assumptions, such as smooth loss landscapes or small weight updates, that may not strictly hold in practical scenarios.

# 3. Preliminaries

#### **Problem Definition**

We consider image classification where the input space  $\mathcal{X}$  is continuous (images) and the label space is discrete  $\mathcal{Y} = \{1,\ldots,K\}$ . Let  $p_{\text{clean}}$  denote the clean data distribution. A (possibly stochastic) corruption kernel  $\kappa(x',y'\mid x,y)$  specifies how a clean pair (x,y) is transformed into a corrupted pair (x',y') if corruption occurs. Pushing  $p_{\text{clean}}$  through  $\kappa$  yields the corrupted distribution

$$p_{\text{corr}}(x', y') = \sum_{y=1}^{K} \int_{\mathcal{X}} p_{\text{clean}}(x, y) \, \kappa(x', y' \mid x, y) \, dx. \quad (1)$$

The observed training distribution by the learning algorithm mixes clean and corrupted distributions, it is formulated as

$$p_{\text{mix}}(\tilde{x}, \tilde{y}) = (1 - \eta) p_{\text{clean}}(\tilde{x}, \tilde{y}) + \eta p_{\text{corr}}(\tilde{x}, \tilde{y}). \tag{2}$$

The training dataset  $\mathcal{D}_{\text{train}} = \{(\tilde{x}_i, \tilde{y}_i)\}_{i=1}^N$  consists of i.i.d. samples drawn from  $p_{mix}$ . Let  $C \subseteq \mathcal{D}_{train}$  denote the subset of corrupted samples. We assume  $\mathcal{D}_{train}$  is inaccessible; instead, we only have access to a proxy dataset  $\mathcal{D}_{proxy} = \{(x'_j, y'_j)\}_{j=1}^M$  drawn exclusively from the corrupted distribution  $p_{corr}$ . The classification problem is modeled by a conditional distribution  $p_{\theta}(y \mid x)$  over  $\mathcal{Y}$ , parameterized by  $\theta \in \Theta \subseteq \mathbb{R}^m$ , and implemented as a neural network  $f: \mathcal{X} \times \Theta \to \mathbb{R}^K$  where  $p_{\theta}(y \mid x) = \operatorname{softmax}(f(x; \theta))_y$ . The model is trained on  $\mathcal{D}_{train}$  to minimize empirical risk with respect to the training samples. Due to overparameterization, the model can achieve near-zero training error, effectively learning/memorizing the corrupted samples. We denote by  $\theta_{mix}$  the resulting parameters after the training is finished. Once learned/memorized, corrupted samples  $\mathcal{C}$  become entangled with clean samples  $\mathcal{S}=\mathcal{D}_{train}\setminus\mathcal{C}$  in the learned representation, and their influence cannot be trivially removed.

Our goal is to transform  $f(\cdot; \theta_{\text{mix}})$ , using only samples in  $\mathcal{D}_{\text{proxy}}$ , into a corrected model  $f(\cdot; \theta_u)$  that approximates an oracle model  $f(\cdot; \theta_{\text{clean}})$  which is trained only on  $\mathcal{S}$ . Let  $\mathcal{U}$  be a post-training corrective method that maps the weights and a set of samples to new weights defined as

$$\mathcal{U}: \Theta \times (\mathcal{X} \times \mathcal{Y})^M \to \Theta, \qquad \theta_u = \mathcal{U}(\theta_{\text{mix}}; \mathcal{D}_{\text{proxy}}).$$
 (3)

The correction is considered to be successful if the predictive distributions of the corrected and oracle models are close in expectation over  $p_{\text{mix}}$ . Specifically, for a choice of pointwise discrepancy  $d(f(x;\theta), f(x;\theta'))$  (e.g., logit MSE) the mismatch between the two models is defined as:

$$\Delta_{\min}(\theta, \theta') := \mathbb{E}_{\tilde{x} \sim p_{\min}}[d(f(\tilde{x}; \theta), f(\tilde{x}; \theta'))]. \tag{4}$$

The goal is then to obtain  $\theta_u = \mathcal{U}(\theta_{\text{mix}}; \mathcal{D}_{\text{proxy}})$  s.t.  $\Delta_{\text{mix}}(\theta_u, \theta_{\text{clean}}) \leq \varepsilon$ , for a small tolerance  $\varepsilon > 0$ .

#### **Corruption Kernels**

Each corruption kernel  $\kappa(x',y'|x,y)$  defines a conditional law over corrupted outputs (x',y') given a clean pair  $(x,y) \sim p_{\text{clean}}$ . For corruptions operating only on labels, inputs remain unchanged, which we express with a Dirac delta  $\delta(x'-x)$ .

**Symmetric Label Noise (SN).** Each clean label is replaced uniformly by a different class. The kernel is

$$\kappa(x', y' \mid x, y) = \delta(x' - x) \frac{\mathbf{1}[y' \neq y]}{K - 1}.$$
 (5)

**Asymmetric Label Noise (AN).** Let  $L \subset \mathcal{Y}$  be the subset of classes that are corrupted, and let  $g:L \to \mathcal{Y}$  be a deterministic mapping with  $g(y) \neq y$  for all  $y \in L$ . The kernel is

$$\kappa(x', y' \mid x, y) = \delta(x' - x) \mathbf{1}[y \in L] \mathbf{1}[y' = g(y)].$$
 (6)

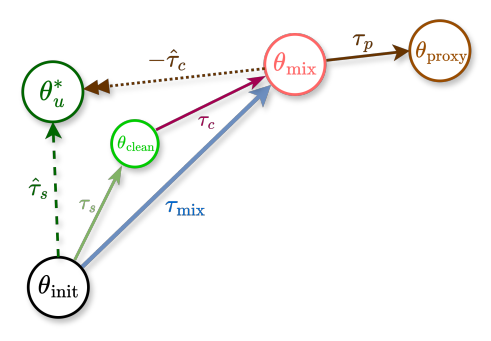


Figure 3. High-level view of CUTS correction procedure in the weight space.

**Poison Trigger (PT).** A trigger operator  $\rho: \mathcal{X} \to \mathcal{X}$  modifies the input, and the label is forced to a target class  $y_t \in \mathcal{Y}$ :

$$\kappa(x', y' \mid x, y) = \delta(x' - \rho(x)) \mathbf{1}[y' = y_t]. \tag{7}$$

# 4. Corrective Unlearning in Task Space

In this section, we introduce our method. The core steps are summarized in Algorithm 1, and an overview of the procedure is shown in Fig. 3.

# Algorithm 1 CUTS algorithm for source-free CMU.

**Input:** Corrupted model  $\theta_{mix}$  trained on partially corrupted training dataset  $\mathcal{D}_{train}{\sim}p_{mix}$ ; proxy dataset  $\mathcal{D}_{\text{proxy}} \sim p_{\text{corr}}$  containing only corrupted samples.

**Post-training Corrective Method** CUTS( $\theta_{mix}$ , $\mathcal{D}_{proxy}$ ):

- 1:  $\theta_{\text{proxy}} = \text{finetune}(\theta_{\text{mix}}, \mathcal{D}_{\text{proxy}})$
- 2:  $\tau_p = \theta_{\text{proxy}} \theta_{\text{mix}}$ 3:  $\hat{\alpha}^* = \text{alpha\_estimator}(\theta_{\text{mix}}, \tau_p, \mathcal{D}_{\text{proxy}})$
- 4:  $\hat{\theta}_u^* = \theta_{\text{mix}} \hat{\alpha}^* \tau_p$
- 5: **return**  $\hat{\theta}_{u}^{*}$

#### Corruption as a Task

Considering the mixture distribution  $p_{mix}$  observed by the learning algorithm, the risk can be decomposed to

$$\mathcal{L}(\theta) = (1 - \eta) \mathbb{E}_{(x,y) \sim p_{\text{clean}}} \left[ \ell(f(x;\theta), y) \right] + \eta \mathbb{E}_{(x',y') \sim p_{\text{corr}}} \left[ \ell(f(x';\theta), y') \right].$$
(8)

We view training on  $\mathcal{D}_{\text{train}} \sim p_{\text{mix}}$  as a multi-task joint learning consisting of two distinct tasks defined by clean samples  $S \sim p_{\text{clean}}$  and corrupted samples  $C \sim p_{\text{corr}}$ .  $T_s$  and  $T_c$  denote the tasks defined by S and C respectively.

The initialization weights for the model are denoted by  $\theta_{\text{init}}$  and the task vector obtained by training on  $\mathcal{D}_{\text{train}}$  is  $\tau_{\rm mix} = \theta_{\rm mix} - \theta_{\rm init}$ . From the task arithmetic perspective,  $\tau_{\rm mix}$ can be decomposed to the summation of two directionally distinct task vectors  $\tau_s$  and  $\tau_c$  associated with  $\mathcal{T}_s$  and  $\mathcal{T}_c$ . That is,  $\tau_{\text{mix}} = \tau_s + \tau_c$ . By estimating  $\tau_c$ , we can recover

the clean task vector by  $\tau_s = \tau_{\rm mix} - \tau_c$  and the clean signal by  $\theta_{\text{clean}} = \theta_{\text{mix}} - \tau_c$ . Intuitively,  $\tau_c$  captures the incremental update in weight space that intensifies the model's reliance on corrupted samples and deviation from the original clean signal. In analogy to how task vectors capture skills or behaviors, here the vector  $\tau_c$  represents the task of "learning corruption". Conversely, going in the negative direction of  $\tau_c$ , would remove these adverse effects from the model.

#### **Source-free Correction**

The original formulation of CMU assumes access to a forget set  $\mathcal{D}_f \subseteq \mathcal{C} \subset \mathcal{D}_{\text{train}}$ , and the goal is to remove the detrimental effect of the corrupted training samples C from the trained weights  $\theta_{\text{mix}}$  using  $\mathcal{D}_f$ , and potentially to use the retain set  $\mathcal{D}_r = \mathcal{D}_{\text{train}} \setminus \mathcal{D}_f$  for preventing damage to clean signal. In the source-free setting we assume access to  $\mathcal{D}_{proxy}$  which serves as a proxy or surrogate for C. We use  $\mathcal{D}_{proxy}$  to define a task  $\mathcal{T}_p$  and the corresponding task vector  $\tau_p$ , which is used to estimate the corruption task vector  $\tau_c$ .

A practical aspect becomes important in the source-free setting. For structured corruptions such as poison triggers, the corruption introduces a consistent and learnable pattern across many samples. As a result, instead of relying on persample memorization, the model can generalize the corruption pattern as if it were a true feature of the data distribution. Such a generalizable feature leads to the transferability of the corruption effect between the learned corrupted training samples and unseen samples in a proxy dataset. That is, if a model is affected by poison triggers, its vulnerability can be observed on the proxy dataset, and if we remove the backdoor, the resulting robustness can also be measured there. Consequently, methods designed to mitigate backdoor corruption on identified poisoned samples in the training dataset tend to exhibit similar effectiveness when applied to a proxy set carrying the same trigger [53]. This, however, contrasts with label noise, where no shared signal exists between corrupted samples, and the only way for the network to fit the corrupted labels is by memorizing individual samples. Therefore, per-sample unlearning methods that target memorized training mistakes tend to be ineffective when applied to a proxy set of corrupted samples never seen by the model during training. We show that despite such fundamental differences between corruption types, it is possible to mitigate their effects through CUTS that operates on the underlying weight space mechanism excited by the corruption, rather than on per-sample associations.

# **Estimation of the Corruption Task Vector**

To estimate  $\tau_c$ , we fine-tune the partially corrupted model  $f(\cdot; \theta_{\text{mix}})$  on the proxy dataset  $\mathcal{D}_{\text{proxy}}$ . This fine-tuning amplifies the corruption patterns already embedded in  $\theta_{\rm mix}$ , producing a model  $f(\cdot; \theta_{proxy})$  that more distinctly reflects corruption-induced behavior. For instance, under symmetric label noise  $f(\cdot; \theta_{proxy})$  behaves nearly as a random classifier, under asymmetric noise it systematically misclassifies corrupted source classes, and under poisoning it becomes more vulnerable to trigger patterns. The weight updates during this process are approximately aligned with the corruption direction defined by  $\tau_c$  rather than the clean signal. We define the corresponding task vector as  $\tau_p = \theta_{\text{proxy}} - \theta_{\text{mix}}$ , which captures the corruption-oriented update induced by proxy fine-tuning. To correct the model, we move from  $\theta_{\text{mix}}$  in the opposite direction of  $\tau_p$ :

$$\theta_u^{\alpha} = \theta_{\text{mix}} - \alpha \, \tau_p, \tag{9}$$

where  $\alpha \geq 0$  controls the strength of the correction; small  $\alpha$  applies a mild adjustment, while larger values more aggressively subtract the corruption component. Next, we define the optimal corrected weights  $\theta_u^* = \theta_{\text{mix}} - \alpha^* \tau_p$  where  $\alpha^*$  is selected to optimize a desired correction objective (e.g., maximizing accuracy on  $\mathcal{D}_{\text{test}}$  or minimizing vulnerability for poison triggers). This choice calibrates the magnitude of the subtraction so that we remove as much of the corruption effect as possible without sacrificing the clean signal. define the estimator  $\hat{\tau}_c = \alpha^* \tau_p$ . In other words,  $\tau_p$  serves as a (approximately) directionally correct proxy for the corruption task vector  $\tau_c$ , and  $\alpha^*$  rescales it to match the strength of the corruption present in  $\theta_{\text{mix}}$ .

#### **Estimating the Optimal Scaling Coefficient**

To eliminate the need for a clean validation dataset, we estimate the optimal scaling coefficient  $\alpha^*$  for the correction operator using only the proxy dataset  $\mathcal{D}_{\text{proxy}} {=} \{(x_i', y_i')\}_{i=1}^M.$  The predicted class for an input  $x_i'$  is denoted by  $\hat{y}_i^\alpha {=} \arg\max_y p^\alpha(y \mid x_i')$  where  $p^\alpha$  denotes the output probabilities by  $\theta_u^\alpha.$  We search over a finite positive grid  $\mathcal{A}$  and denote the resulting estimator by  $\hat{\alpha}^*$  and the corrected weights by this estimator by  $\hat{\theta}_u^*$  (CUTS).

**Poison triggers.** For the poison triggers, we measure the attack success rate (ASR) of  $\theta_u^{\alpha}$  on  $\mathcal{D}_{\text{proxy}}$  and choose the smallest update that reliably suppresses the backdoor

$$\hat{\alpha}^* = \min \left\{ \alpha \in \mathcal{A} : \underbrace{\frac{1}{M} \sum_{i=1}^{M} \mathbf{1} [\hat{y}_i^{\alpha} = y_t]}_{\text{ASR}(\alpha)} \le \varepsilon \right\}. \tag{10}$$

with a small threshold  $\varepsilon$  (we use  $\varepsilon = 0.01$ ).

**Symmetric/asymmetric label noise.** In the case of symmetric and asymmetric label noise a targeted behavior which can be evaluated directly on the samples of  $\mathcal{D}_{\text{proxy}}$  is not present. Empirically, such noise collapses and overlaps class clusters in the penultimate representation. We therefore use an unsupervised kNN self-agreement criterion on the input images  $\{x_i'\}$  in the proxy dataset.

Let  $h_i$  be the L2-normalized version of feature outputted by the penultimate embedding of  $f(x_i'; \theta_u^{\alpha})$ . Let  $\mathcal{N}_k(i)$  be the indices of the k nearest neighbors of  $h_i$  (Euclidean distance). The aggregated self-agreement score is

$$SA(\alpha) = \frac{1}{N} \sum_{i=1}^{N} \frac{1}{k} \sum_{j \in \mathcal{N}_k(i)} \mathbf{1} \left[ \hat{y}_j^{\alpha} = \hat{y}_i^{\alpha} \right]. \tag{11}$$

 $\mathrm{SA}(\alpha)$  increases when clusters become tighter and more separated, and decreases when clusters overlap or fragment. To prevent models that predict only a few classes for all samples from achieving a high kNN self-agreement, we penalize the agreement scores by a coverage term which forces the estimator to eliminate falsely corrected models. Considering the number of clusters  $|\mathcal{Y}|$  and a coverage rate  $\rho \in (0,1]$ , which is a hyperparameter depending on the size of proxy dataset, we require only  $r = \lceil \rho |\mathcal{Y}| \rceil$  clusters to be sufficiently represented (support at least k+1 samples). Let  $V(\alpha)$  be the number of predicted classes meeting this support; we estimate the optimal scaling coefficient as

$$\hat{\alpha}^* = \underset{\alpha \in \mathcal{A}}{\arg \max} \left[ SA(\alpha) - \frac{\max\{0, r - V(\alpha)\}}{r} \right]. \quad (12)$$

#### **Evaluation Metrics**

For label corruption, the goal of correction is to maximize generalization. We report Utility (UT%) as the classification accuracy on the clean test dataset  $\mathcal{D}_{\text{test}}$ . To quantify how much of the gap between the corrupted model  $\theta_{\text{mix}}$  and the oracle  $\theta_{\text{clean}}$  is closed by a corrected model  $\theta_u$ , we use the Recovery Rate (RR%) defined as

$$RR(\theta_u) = \frac{UT(\theta_u) - UT(\theta_{mix})}{UT(\theta_{clean}) - UT(\theta_{mix})}.$$
 (13)

For poison triggers, a successful correction must remove the trigger effect while preserving utility. We measure the trigger effect with the Attack Success Rate (ASR%), the percentage of triggered samples in  $\mathcal{C}$  that are classified as the attacker's target label. Lower is better. We also report an overall score for poison unlearning called Poison Unlearning Score (PUS%),

$$PUS(\theta_u) = UT(\theta_u) \times (100 - ASR(\theta_u))/100.$$
 (14)

# 5. Experiments

Datasets, corruption injection, and models. We evaluate CUTS on three benchmark datasets MNIST [36] and CIFAR10/100 [34] and on Clothing1M [67], a real-world noisy dataset. For experiments involving synthetic corruptions, unless stated otherwise, we hold out 2% of the original training split as  $\mathcal{D}_{proxy}$ , before injecting corruption. Then we inject corruption at rate  $\eta$  only into the remaining training split to create  $\mathcal{D}_{train}$ . All of the samples in  $\mathcal{D}_{proxy}$  are then corrupted with the same corruption kernel as for  $\mathcal{D}_{train}$ . For corruption types which do not operate on all classes, we

Table 1. Results for CLIP models trained under symmetric (SN) and asymmetric (AN) label noise. Cell values show the utility (UT%).
The rightmost column reports the average recovery rate (RR%). Best results are shown in bold; second-best results are underlined.

			MNIST	Γ				(	CIFAR1	0					C	IFAR1	00			Avg.
			SN					SN			A	.N			SN			A	.N	RR
Model	10%	20%	40%	60%	80%	10%	20%	40%	60%	80%	20%	40%	10%	20%	40%	60%	80%	20%	40%	
Mix Oracle	98.7 99.7	96.0 99.7	81.7 99.7	57.1 99.6	24.8 99.5	96.9 98.6	93.5 98.7	76.2 98.5	51.9 98.4	22.7 98.0	94.7 98.7	83.1 98.4	88.2 90.2	84.6 90.2	72.5 89.8		24.9 86.9	80.9 90.2	60.5 89.4	0.0
$Mix- au_r$ SAP CF	98.7 99.3 <b>99.4</b>	96.1 98.6 98.9	81.8 95.0 97.7	57.1 92.0 96.6	25.2 58.4 <b>94.0</b>	96.8 97.0 97.5	93.5 95.1 <b>97.1</b>	85.0	52.0 72.0 <b>94.2</b>	26.3	94.7 95.2 97.2	83.1 81.4 <b>96.4</b>	88.2 88.1 87.1		72.4 75.8 82.7	52.0 59.4 <b>80.0</b>	24.7 28.5 <b>74.3</b>	80.9 81.3 86.2	60.6 61.5 <b>82.8</b>	
CUTS	99.4 99.4		98.0	96.8	<u>84.9</u>	97.3 <b>97.7</b>	97.1 97.0	95.5 95.5	91.8 91.8	80.9	97.4	95.5		86.8	83.1	78.3	64.9	86.3	82.2	69.4

only keep the samples that get corrupted by the corruption kernel in the proxy dataset. For symmetric noise we inject corruption at rates  $\eta \in \{10\%, 20\%, 40\%, 60\%, 80\%\}$  and for asymmetric noise at  $\eta \in \{20\%, 40\%\}$  using dataset-specific mappings g(y) following [40]. Poison trigger is injected at  $\eta \in \{2\%, 10\%, 20\%\}$ . Following [23], we adopt a BadNetsstyle trigger [25] by whitening 3% of the bottom-right pixels and assigning class 0 to triggered samples.

We use a pre-trained CLIP vision encoder (ViT-B/16) [52] as is common in task arithmetic studies. For MNIST, we additionally include a fully connected network with one hidden layer of dimension 32,768 (FC1). For CI-FAR10/100, we further consider ResNet18/34/50/101 [28] models with both random initialization and ImageNet-pretrained weights. We also perform experiments on DINOv3 (ViT-B/16-distilled) [55] backbone, and vanilla ViT (ViT-B/16) [14]. We report the results for DINOv3, vanilla ViT, and additional  $\eta$  values for ResNets in Sec. B.

**Baselines and training.** The **Mix** model ( $\theta_{mix}$ ) defines the base performance, while the **Oracle** ( $\theta_{clean}$ ) is obtained by training  $\theta_{\text{init}}$  on the clean set S and serves as an upper bound for any corrective unlearning method. To demonstrate the effectiveness of our method we employ several baselines. For label corruption, we compare against **SAP** [33], the current SOTA CMU method under label noise, which operates on a small set of clean samples (those not memorized under noisy labels during training). For poison triggers, we use **Potion** [53], a SOTA poison unlearning method operating only on a forget set. We also consider a catastrophic forgetting baseline CF [22], where we fine-tune  $\theta_{mix}$  on a set of clean samples to induce forgetting of corruption effect. For fair comparison, both SAP and CF use a clean version of  $\mathcal{D}_{proxy}$  (no injected corruption), whereas CUTS and Potion are applied on corrupted  $\mathcal{D}_{proxy}$ . Neither SAP nor Potion uses the retain set  $\mathcal{D}_r$ , so all methods can be evaluated in the same source-free setting. Note that obtaining clean samples can be substantially more costly than assembling corrupted proxies; for instance, under symmetric label noise one can form  $\mathcal{D}_{\text{proxy}}$  by taking diverse images and assigning random labels, whereas acquiring their correct labels requires additional annotation effort. Finally, to control for the possibility that improvements arise from generic parameter perturbations rather than targeted negation, we include a random task vector baseline  $\mathbf{Mix} - \tau_r$ , where  $\tau_r$  matches the layerwise norm of  $\hat{\tau}_c$  as proposed by [30].

Across all experiments, we pre-train and fine-tune models using cross-entropy loss and continue training until (near) 100% training accuracy is reached. This is crucial in the presence of corruption as stopping early would implicitly act as regularization and prevent the full effect of corruption from manifesting in the model. To obtain the mixed weights  $\theta_{\text{mix}}$ , we train the model from  $\theta_{\text{init}}$  (either pre-trained or randomly initialized, depending on the experiment) on  $\mathcal{D}_{\text{train}}$ . We then fine-tune  $\theta_{\text{mix}}$  on  $\mathcal{D}_{\text{proxy}}$  to obtain  $\theta_{\text{proxy}}$ . The scaling coefficient  $\hat{\alpha}^*$  for CUTS is selected from a grid  $\mathcal{A}=\{0.05,\,0.1,\,\ldots,\,4.0\}$ . Further training details and hyperparameters are reported in Sec. A.

# 5.1. Results

**Label noise.** Table 1 reports the results for CLIP models under label noise. Moving along the direction of a random vector  $\tau_r$  in the weight space fails to remove the corruption, indicating that the direction of the edit is important. CUTS consistently recovers a large fraction of the gap between Mix and Oracle models and the average recovery is higher than CF (which operates on fully clean labels). Much to our surprise, SAP fails to provide comparable performance with the simple baseline CF (both operating on clean samples). We hypothesize that SAP relies heavily on the samples used to project activations being low loss samples, which cannot be identified in the source-free setting. Table 2 shows the results for randomly initialized networks trained under label noise. We observed that correction is essentially harder (lower RR for all methods) when networks are initialized randomly (before training on  $\mathcal{D}_{train}$ ) rather than with pretrained priors. In Section 5.2, we analyze the effect of pretrained priors on the effectiveness of CUTS.

Table 2. Utility (UT%) for randomly initialized models trained under symmetric (SN) and asymmetric (AN) label noise. FC1 is a fully connected network; R18 is ResNet-18. Last column gives average recovery rate (RR%). Best in bold; second-best underlined.

	MN	IST +	FC1	CIFA	AR10 +	R18	CIFA	R100 -	+ R18	Avg.
	S	N	AN	S	N	AN	S	N	AN	RR
Model	20%	40%	40%	20%	40%	40%	20%	40%	40%	
Mix Oracle	92.9 98.4	79.7 98.3	81.9 98.3	77.9 88.9	60.0 87.4	74.5 88.7	52.6 66.9	38.3 63.9	41.5 63.9	0.0
$Mix- au_r$ SAP CF CUTS	91.9 <b>96.4</b> 94.9 95.0	79.0 <b>93.8</b> 91.1 93.6	81.9 86.9 90.9 <b>93.6</b>	66.0 81.2 80.0 <b>81.2</b>	9.9 <u>67.1</u> <b>69.2</b> 65.8	24.3 75.0 <b>80.0</b> 79.8	1.2 53.1 <u>53.5</u> <b>54.4</b>	1.0 40.7 41.8 <b>42.1</b>	1.5 42.0 <b>45.8</b> 44.5	-150.0 27.2 31.3 34.7

**Poison trigger.** The results of applying the corrective methods under poison trigger corruption for CLIP are summarized in Tab. 3. Unlike label noise, backdoor triggers introduce learnable features in the input, which the model learns and associates with the target class. This explains why CF generally fails to remove the trigger; the backdoor feature does not significantly degrade clean signal utility (as indicated by the UT% of the Mix model), and brief finetuning on the clean task cannot undo the feature—target association. In contrast, our method reliably eliminates the trigger while outperforming the SOTA poison unlearning method Potion. Notably, Potion collapses when the corruption rate is high, whereas CUTS shows stronger robustness and can remove the trigger using a proxy set with only one-tenth the size of  $\mathcal{C}$ .

Table 3. Results for CLIP trained under poison trigger corruption. Columns show utility (UT%) and attack success rate (ASR%). The right most column shows the average poison unlearning score (PUS). Best results (PUS) are in bold; second-best are underlined.

				CIF	AR10					CIFA	R100			Avg.
		29	%	10	)%	20	)%	2	%	10	)%	20	)%	PUS
Model	U.	Γ	ASR	UT	ASR	UT	ASR	UT	ASR	UT	ASR	UT	ASR	
Mix Oracle											100 0.0			0.0 94.5
$Mix- au_r$ CF Potion CUTS	97. <b>98.</b>	.8 . <b>4</b>	100 <b>0.9</b>	97.9 10.5	100 <u>0.5</u>	97.9 10.4	100 <u>0.4</u>	99.6 <u>87.8</u>	100 <u>1.0</u>	89.1 73.5	100 100 <u>0.7</u> <b>1.6</b>	88.5 <u>49.4</u>	100 1.2	0.0 0.0 54.5 <b>90.3</b>

**Real-world dataset.** We tested CUTS on Clothing1M [67], a real-world noisy dataset. For the proxy dataset, we randomly sampled 1000 images from the validation set and corrupted their labels with symmetric noise. Although the original dataset may involve a more complex noise transition matrix, we assume it is unknown and use the symmetric noise (one can use noise transition matrix estimation methods for better results). We trained a classifier with DINOv3 backbone to reach near perfect training accuracy (99.89%).

Table 4. Results on DINOv3 trained on Clothing1M, averaged over 4 runs with different proxy draws and noise seeds.

Model	UT	Improvement
Mix	66.42	-
$\text{Mix}- au_r$	$66.47 \pm 0.03$	0.05
CF	$\textbf{71.64} \pm \textbf{0.26}$	5.22
CUTS	$69.26 \pm 0.85$	2.84

The results of correction are summarized in Tab. 4; CUTS recovers an average of 2.84% utility over Mix.

# 5.2. Ablation and Analysis

This section presents the main ablation studies; additional analyses including the effect of the size of  $\mathcal{D}_{proxy}$  and the cosine similarity between task vectors are reported in Sec. C.

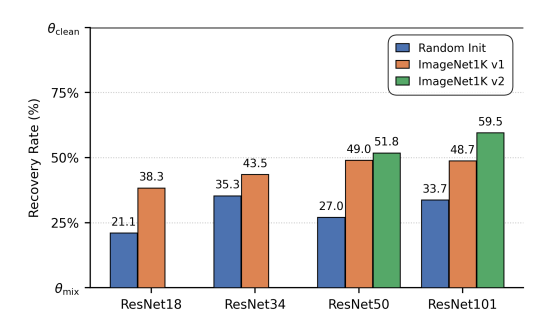


Figure 4. RR% of CUTS on ResNet models with different initializations on CIFAR10 with symmetric label noise at  $\eta$ =40%.

**Pre-trained priors.** Task arithmetic is most reliable when the network exhibits weight disentanglement and this disentanglement is an emergent property of large pre-training rather than a generic property of neural networks [50]. Figure 4 illustrates the effect of pre-trained priors on the effectiveness of CUTS for ResNet models initialized randomly and with ImageNet1K weights. We observe that better pre-training leads to better disentanglement of the directions associated with corruption and clean tasks in the weight space, which directly impact the performance of CUTS.

**PCA trajectory.** In order to analyze how CUTS alters the corrupted model, we inspect the embedding space by applying PCA to the penultimate features of  $\theta_{\rm mix} - \alpha \tau_p$ , varying  $\alpha \in \{0, \hat{\alpha}^*/3, 2\hat{\alpha}^*/3, \hat{\alpha}^*\}$ . Results are shown in Fig. 5. For label noise, class embeddings are initially collapsed/overlapping due to the high fraction of noisy labels, and increasing the correction strength (i.e. gradually increasing  $\alpha$ ) progressively separates the class clusters and partially restores the decision boundaries. For poison trigger, the triggered inputs are mapped to a compact cluster

that is distinct from clean samples of the same target class. As  $\alpha$  increases, this triggered cluster dissolves and the samples migrate into their true class clusters.

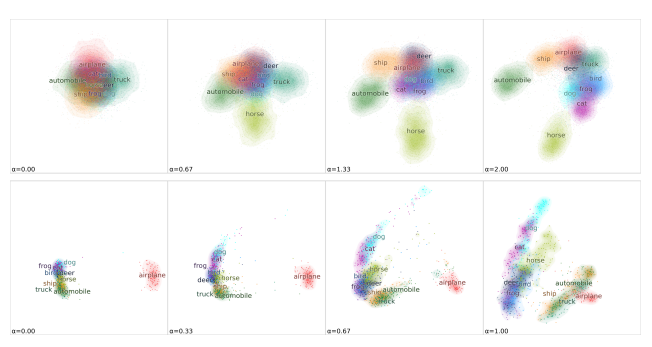


Figure 5. PCA of the penultimate features of CLIP for  $\theta_{\rm mix} - \alpha \tau_p$ , varying  $\alpha \in \{0, \hat{\alpha}^*/3, 2\hat{\alpha}^*/3, \hat{\alpha}^*\}$ . Top: CIFAR10 under symmetric label noise at  $\eta$ =60%. Bottom: CIFAR10 under poison trigger corruption at  $\eta$ =2% with target class airplane.

Correcting "clean" samples in the original dataset. As correction progresses along the correction ray  $-\tau_p$  by increasing  $\alpha$ , in addition to forgetting samples from  $\mathcal{C}$ , the model also gradually changes its prediction on a number of samples in  $\mathcal{S}$ . By inspecting these samples (as shown in Fig. 6), we observed that many of the earliest "clean" flips are either mislabeled and ambiguous or atypical and low-support instances that sit near the decision boundaries.



Figure 6. Clean training samples that flip first when increasing  $\alpha$  along  $-\tau_p$  for CLIP trained under symmetric label noise at  $\eta$ =10%. Captions show *ground truth*  $\rightarrow$  *predicted*.

Interpolation along  $\tau_{mix}$  and post-training early stopping. Studies have shown that during empirical risk minimization, neural networks tend to learn simple and frequent patterns first, which usually correspond to clean and easy examples, and only later in the training, begin to memorize rare, hard, and noisy samples [1, 45, 47]. Despite this ordering, the training trajectory in weight space is often highly nonlinear for randomly initialized models. For pre-trained models, however, fine-tuning tends to move in a lower dimensional and more linearly connected region of the loss

landscape [15, 20, 30, 65]. We tested whether the approximately linear behavior often seen during fine-tuning also appears when the training data are partially corrupted, and whether it aligns with the "simple to noisy" learning order described. To do so, we interpolated along  $au_{
m mix}$  and evaluated each model on  $\mathcal{D}_{test}$ ,  $\mathcal{S}$ , and  $\mathcal{C}$ . As shown in Fig. 7, as the model moves from  $\theta_{\text{init}}$  to  $\theta_{\text{mix}}$  along  $\tau_{\text{mix}}$ , accuracy on S increases first while accuracy on C stays low, which leads to a rise in test accuracy. After the clean samples are largely fit, the model begins to fit noisy samples and test accuracy begins to drop. These results are consistent with an approximately linear fine-tuning path for pre-trained models even under substantial label noise and with the known training time ordering where clean examples are learned before noisy ones. Practically, this unlocks a simple post-training early stopping possibility. One can sweep the interpolation coefficient along  $au_{mix}$  and pick the point that maximizes validation accuracy, which can recover the best generalization without rerunning training (in case  $\theta_{init}$  are available).

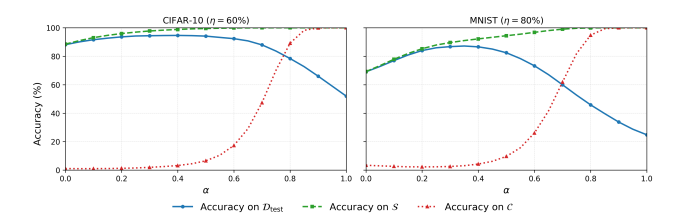


Figure 7. Accuracy of the interpolated CLIP models along  $\tau_{\rm mix}$  on test dataset and clean and noisy splits ( $\mathcal S$  and  $\mathcal C$ ) of the training datasets of CIFAR-10 and MNIST under symmetric label noise.

#### 6. Conclusion

In this work, we formalized source-free CMU, which tackles a realistic problem where training data is not available for correction, and introduced CUTS which applies CMU using a small set of corrupted samples which do not need to be from the training set of the model. Particularly, we treat corruption as a task in the task space and operate on task directions in the weight space instead of per-sample associations. We also showed the effect of pre-trained priors on disentanglement of the clean and corruption tasks in the weight space. CUTS gains on randomly initialized networks are smaller which is in parallel with previous observations in task arithmetic works [50]. One possible extension of our work can be a zero-shot version of CMU, where the proxy set is generated directly from the trained models using data-free inversion methods [9, 70]. Scaling coefficient  $\alpha$  can also be tuned layer-wise instead of a single global coefficient.

#### References

- [1] Devansh Arpit, Stanisław Jastrzebski, Nicolas Ballas, David Krueger, Emmanuel Bengio, Maxinder S. Kanwal, Tegan Maharaj, Asja Fischer, Aaron Courville, Yoshua Bengio, and Simon Lacoste-Julien. A closer look at memorization in deep networks. In *ICML*, pages 233–242, 2017. 1, 2, 8
- [2] Heesun Bae, Seungjae Shin, Byeonghu Na, Joonho Jang, Kyungwoo Song, and Il-Chul Moon. From noisy prediction to true label: Noisy prediction calibration via generative model. In *ICML*, pages 1277–1297, 2022. 1
- [3] Robert John Nicholas Baldock, Hartmut Maennel, and Behnam Neyshabur. Deep learning through the lens of example difficulty. In *NeurIPS*, 2021. 2
- [4] Marco Barreno, Blaine Nelson, Russell Sears, Anthony D. Joseph, and J. D. Tygar. Can machine learning be secure? In *Proceedings of the 2006 ACM Symposium on Information, Computer and Communications Security*, 2006. 1
- [5] Abeba Birhane and Vinay Uday Prabhu. Large image datasets: A pyrrhic win for computer vision? In *IEEE Winter Conference on Applications of Computer Vision (WACV)*, pages 1536–1546, 2021. 1
- [6] Lucas Bourtoule, Varun Chandrasekaran, Christopher A. Choquette-Choo, Hengrui Jia, Adelin Travers, Baiwu Zhang, David Lie, and Nicolas Papernot. Machine unlearning, 2020. 1, 2
- [7] Yinzhi Cao and Junfeng Yang. Towards making systems forget with machine unlearning. In *IEEE Symposium on Security and Privacy (SP)*, pages 463–480, 2015. 2
- [8] Nicholas Carlini, Matthew Jagielski, Christopher A. Choquette-Choo, Daniel Paleka, Will Pearce, Hyrum Anderson, Andreas Terzis, Kurt Thomas, and Florian Tramer. Poisoning web-scale training datasets is practical. In *IEEE Symposium on Security and Privacy (SP)*, pages 407–425, 2024. 1
- [9] Hanting Chen, Yunhe Wang, Chang Xu, Zhaohui Yang, Chuanjian Liu, Boxin Shi, Chunjing Xu, Chao Xu, and Qi Tian. Data-free learning of student networks. In *ICCV*, pages 3513–3521, 2019. 8
- [10] Xinyun Chen, Chang Liu, Bo Li, Kimberly Lu, and Dawn Xiaodong Song. Targeted backdoor attacks on deep learning systems using data poisoning. *arXiv preprint arXiv:1712.05526*, 2017. 1
- [11] Yanjiao Chen, Xueluan Gong, Qian Wang, Xing Di, and Huayang Huang. Backdoor attacks and defenses for deep neural networks in outsourced cloud environments. *IEEE Network*, 34(5):141–147, 2020. 1
- [12] Hao Cheng, Zhaowei Zhu, Xingyu Li, Yifei Gong, Xing Sun, and Yang Liu. Learning with instance-dependent label noise: A sample sieve approach. In *ICLR*, 2021. 1
- [13] Vikram S Chundawat, Ayush K Tarun, Murari Mandal, and Mohan Kankanhalli. Can bad teaching induce forgetting? unlearning in deep networks using an incompetent teacher. In AAAI, 2023. 3
- [14] Alexey Dosovitskiy, Lucas Beyer, Alexander Kolesnikov, Dirk Weissenborn, Xiaohua Zhai, Thomas Unterthiner, Mostafa Dehghani, Matthias Minderer, Georg Heigold, Sylvain Gelly, Jakob Uszkoreit, and Neil Houlsby. An image is

- worth 16x16 words: Transformers for image recognition at scale. In *ICLR*, 2021. 6
- [15] Felix Draxler, Kambis Veschgini, Manfred Salmhofer, and Fred Hamprecht. Essentially no barriers in neural network energy landscape. In *ICML*, pages 1309–1318, 2018. 8
- [16] Vitaly Feldman. Does learning require memorization? a short tale about a long tail, 2021. 2
- [17] Vitaly Feldman and Chiyuan Zhang. What neural networks memorize and why: Discovering the long tail via influence estimation, 2020. 2
- [18] Jack Foster, Stefan Schoepf, and Alexandra Brintrup. Fast machine unlearning without retraining through selective synaptic dampening. *Proceedings of the AAAI Conference* on Artificial Intelligence, 38(11):12043–12051, 2024. 3
- [19] Benoit Frenay and Michel Verleysen. Classification in the presence of label noise: A survey. *IEEE Transactions* on Neural Networks and Learning Systems, 25(5):845–869, 2014. 1
- [20] Timur Garipov, Pavel Izmailov, Dmitrii Podoprikhin, Dmitry Vetrov, and Andrew Gordon Wilson. Loss surfaces, mode connectivity, and fast ensembling of dnns. In *NeurIPS*, pages 8803–8812, 2018. 8
- [21] Antonio Ginart, Melody Y. Guan, Gregory Valiant, and James Zou. Making ai forget you: Data deletion in machine learning, 2019. 1, 2
- [22] Shashwat Goel, Ameya Prabhu, Amartya Sanyal, Ser-Nam Lim, Philip Torr, and Ponnurangam Kumaraguru. Towards adversarial evaluations for inexact machine unlearning, 2023. 3, 6
- [23] Shashwat Goel, Ameya Prabhu, Philip Torr, Ponnurangam Kumaraguru, and Amartya Sanyal. Corrective machine unlearning, 2024. 1, 2, 3, 6
- [24] Aditya Golatkar, Alessandro Achille, and Stefano Soatto. Eternal sunshine of the spotless net: Selective forgetting in deep networks, 2020. 2
- [25] Tianyu Gu, Kang Liu, Brendan Dolan-Gavitt, and Siddharth Garg. Badnets: Evaluating backdooring attacks on deep neural networks. *IEEE Access*, 7:47230–47244, 2019. 2, 6
- [26] Chuan Guo, Tom Goldstein, Awni Hannun, and Laurens Van Der Maaten. Certified data removal from machine learning models. In *ICML*. JMLR.org, 2020. 1, 2
- [27] Bo Han, Quanming Yao, Xingrui Yu, Gang Niu, Miao Xu, Weihua Hu, Ivor W. Tsang, and Masashi Sugiyama. Coteaching: robust training of deep neural networks with extremely noisy labels. In *NeurIPS*, pages 8536–8546, 2018.
- [28] Kaiming He, Xiangyu Zhang, Shaoqing Ren, and Jian Sun. Deep residual learning for image recognition. In *CVPR*, pages 770–778, 2016. 6
- [29] Kunzhe Huang, Yiming Li, Baoyuan Wu, Zhan Qin, and Kui Ren. Backdoor defense via decoupling the training process. In *ICLR*, 2022. 1
- [30] Gabriel Ilharco, Marco Tulio Ribeiro, Mitchell Wortsman, Ludwig Schmidt, Hannaneh Hajishirzi, and Ali Farhadi. Editing models with task arithmetic. In *ICLR*, 2023. 2, 3, 6, 8

- [31] Leonardo Iurada, Marco Ciccone, and Tatiana Tommasi. Efficient model editing with task-localized sparse fine-tuning. In *ICLR*, 2025. 2, 3
- [32] Taehyeon Kim, Jongwoo Ko, Sangwook Cho, Jinhwan Choi, and Se-Young Yun. Fine samples for learning with noisy labels. In *NeurIPS*, 2021.
- [33] Sangamesh Kodge, Deepak Ravikumar, Gobinda Saha, and Kaushik Roy. Sap: Corrective machine unlearning with scaled activation projection for label noise robustness, 2024. 3, 6
- [34] Alex Krizhevsky. Learning multiple layers of features from tiny images. Technical report, University of Toronto, 2009. Technical Report. 5
- [35] Meghdad Kurmanji, Peter Triantafillou, Jamie Hayes, and Eleni Triantafillou. Towards unbounded machine unlearning. In *NeurIPS*, 2023. 3
- [36] Yann LeCun, Léon Bottou, Yoshua Bengio, and Patrick Haffner. Gradient-based learning applied to document recognition. *Proceedings of the IEEE*, 86(11):2278–2324, 1998.
- [37] Hongkang Li, Yihua Zhang, Shuai Zhang, Pin-Yu Chen, Sijia Liu, and Meng Wang. When is task vector provably effective for model editing? a generalization analysis of nonlinear transformers. In *ICLR*, 2025. 2, 3
- [38] Yige Li, Xixiang Lyu, Nodens Koren, Lingjuan Lyu, Bo Li, and Xingjun Ma. Anti-backdoor learning: training clean models on poisoned data. In *NeurIPS*, 2021. 1
- [39] Sheng Liu, Jonathan Niles-Weed, Narges Razavian, and Carlos Fernandez-Granda. Early-learning regularization prevents memorization of noisy labels. In *NeurIPS*, 2020. 1
- [40] Sheng Liu, Zhihui Zhu, Qing Qu, and Chong You. Robust training under label noise by over-parameterization. In *ICML*, pages 14153–14172, 2022. 2, 6
- [41] Yingqi Liu, Shiqing Ma, Yousra Aafer, Wen-Chuan Lee, Juan Zhai, Weihang Wang, and X. Zhang. Trojaning attack on neural networks. In *Network and Distributed System Security Symposium (NDSS)*, 2018. 1
- [42] Ilya Loshchilov and Frank Hutter. SGDR: Stochastic gradient descent with warm restarts. In *ICLR*, 2017. 1
- [43] Ilya Loshchilov and Frank Hutter. Decoupled weight decay regularization. In *ICLR*, 2019.
- [44] Xingjun Ma, Hanxun Huang, Yisen Wang, Simone Romano Sarah Erfani, and James Bailey. Normalized loss functions for deep learning with noisy labels. In *ICML*, 2020. 1
- [45] Pratyush Maini, Michael C. Mozer, Hanie Sedghi, Zachary C. Lipton, J. Zico Kolter, and Chiyuan Zhang. Can neural network memorization be localized?, 2023. 2, 8
- [46] Eran Malach and Shai Shalev-Shwartz. Decoupling "when to update" from "how to update". In *NeurIPS*, pages 961–971, 2017.
- [47] Preetum Nakkiran, Gal Kaplun, Dimitris Kalimeris, Tristan Yang, Benjamin L. Edelman, Fred Zhang, and Boaz Barak. Sgd on neural networks learns functions of increasing complexity, 2019. 8
- [48] Tuan Anh Nguyen and Anh Tuan Tran. Wanet imperceptible warping-based backdoor attack. In *ICLR*, 2021. 1

- [49] Curtis G Northcutt, Anish Athalye, and Jonas Mueller. Pervasive label errors in test sets destabilize machine learning benchmarks. In *NeurIPS*, 2021. 1
- [50] Guillermo Ortiz-Jimenez, Alessandro Favero, and Pascal Frossard. Task arithmetic in the tangent space: Improved editing of pre-trained models. In *NeurIPS*, 2023. 2, 3, 7, 8
- [51] Adam Paszke, Sam Gross, Francisco Massa, Adam Lerer, James Bradbury, Gregory Chanan, Trevor Killeen, Zeming Lin, Natalia Gimelshein, Luca Antiga, Alban Desmaison, Andreas Köpf, Edward Yang, Zachary DeVito, Martin Raison, Alykhan Tejani, Sasank Chilamkurthy, Benoit Steiner, Lu Fang, Junjie Bai, and Soumith Chintala. Pytorch: An imperative style, high-performance deep learning library. arXiv preprint arXiv:1912.01703, 2019. 1
- [52] Alec Radford, Jong Wook Kim, Chris Hallacy, Aditya Ramesh, Gabriel Goh, Sandhini Agarwal, Girish Sastry, Amanda Askell, Pamela Mishkin, Jack Clark, Gretchen Krueger, and Ilya Sutskever. Learning transferable visual models from natural language supervision, 2021. 6
- [53] Stefan Schoepf, Jack Foster, and Alexandra Brintrup. Potion: Towards poison unlearning. *Journal of Data-centric Machine Learning Research*, 2024. 3, 4, 6
- [54] Stefan Schoepf, Michael Curtis Mozer, Nicole Elyse Mitchell, Alexandra Brintrup, Georgios Kaissis, Peter Kairouz, and Eleni Triantafillou. Redirection for erasing memory (rem): Towards a universal unlearning method for corrupted data, 2025. 2, 3
- [55] Oriane Siméoni, Huy V. Vo, Maximilian Seitzer, Federico Baldassarre, Maxime Oquab, Cijo Jose, Vasil Khalidov, Marc Szafraniec, Seungeun Yi, Michaël Ramamonjisoa, Francisco Massa, Daniel Haziza, Luca Wehrstedt, Jianyuan Wang, Timothée Darcet, Théo Moutakanni, Leonel Sentana, Claire Roberts, Andrea Vedaldi, Jamie Tolan, John Brandt, Camille Couprie, Julien Mairal, Hervé Jégou, Patrick Labatut, and Piotr Bojanowski. Dinov3, 2025. 6
- [56] Hwanjun Song, Minseok Kim, Dongmin Park, Yooju Shin, and Jae-Gil Lee. Learning from noisy labels with deep neural networks: A survey, 2022. 1
- [57] Jacob Steinhardt, Pang Wei Koh, and Percy Liang. Certified defenses for data poisoning attacks. In *NeurIPS*, pages 3520– 3532, 2017. 1
- [58] Cory Stephenson, Suchismita Padhy, Abhinav Ganesh, Yue Hui, Hanlin Tang, and SueYeon Chung. On the geometry of generalization and memorization in deep neural networks, 2021. 2
- [59] Daiki Tanaka, Daiki Ikami, Toshihiko Yamasaki, and Kiyoharu Aizawa. Joint optimization framework for learning with noisy labels. In CVPR, pages 5552–5560, 2018.
- [60] Brandon Tran, Jerry Li, and Aleksander Madry. Spectral signatures in backdoor attacks. In *NeurIPS*, pages 8011– 8021, 2018. 1
- [61] Weiqi Wang, Zhiyi Tian, Chenhan Zhang, and Shui Yu. Machine unlearning: A comprehensive survey, 2024. 2
- [62] Yisen Wang, Xingjun Ma, Zaiyi Chen, Yuan Luo, Jinfeng Yi, and James Bailey. Symmetric cross entropy for robust learning with noisy labels. In *ICCV*, pages 322–330, 2019. 1
- [63] Farooq Ahmad Wani, Maria Sofia Bucarelli, and Fabrizio Silvestri. Learning with noisy labels through learnable

- weighting and centroid similarity. In *International Joint Conference on Neural Networks (IJCNN)*, pages 1–9, 2024.
- [64] Hongxin Wei, Lei Feng, Xiangyu Chen, and Bo An. Combating noisy labels by agreement: A joint training method with co-regularization. In CVPR, pages 13723–13732, 2020.
- [65] Mitchell Wortsman, Gabriel Ilharco, Samir Ya Gadre, Rebecca Roelofs, Raphael Gontijo-Lopes, Ari S Morcos, Hongseok Namkoong, Ali Farhadi, Yair Carmon, Simon Kornblith, and Ludwig Schmidt. Model soups: averaging weights of multiple fine-tuned models improves accuracy without increasing inference time. In *ICML*, pages 23965–23998, 2022. 8
- [66] Xiaobo Xia, Tongliang Liu, Bo Han, Chen Gong, Nannan Wang, Zongyuan Ge, and Yi Chang. Robust early-learning: Hindering the memorization of noisy labels. In *ICLR*, 2021.
- [67] Tong Xiao, Tian Xia, Yi Yang, Chang Huang, and Xiaogang Wang. Learning from massive noisy labeled data for image classification. In CVPR, 2015. 5, 7
- [68] Jie Xu, Zihan Wu, Cong Wang, and Xiaohua Jia. Machine unlearning: Solutions and challenges. *IEEE Transactions* on Emerging Topics in Computational Intelligence, 8:2150– 2168, 2023. 2
- [69] Yu Yao, Tongliang Liu, Bo Han, Mingming Gong, Jiankang Deng, Gang Niu, and Masashi Sugiyama. Dual t: reducing estimation error for transition matrix in label-noise learning. In *NeurIPS*, 2020. 1
- [70] Hongxu Yin, Pavlo Molchanov, Jose M. Alvarez, Zhizhong Li, Arun Mallya, Derek Hoiem, Niraj K Jha, and Jan Kautz. Dreaming to distill: Data-free knowledge transfer via deepinversion. In CVPR, 2020. 8
- [71] Siqi Zeng, Yifei He, Weiqiu You, Yifan Hao, Yao-Hung Hubert Tsai, Makoto Yamada, and Han Zhao. Efficient model editing with task vector bases: A theoretical framework and scalable approach, 2025. 2, 3
- [72] Chiyuan Zhang, Samy Bengio, Moritz Hardt, Benjamin Recht, and Oriol Vinyals. Understanding deep learning (still) requires rethinking generalization. *Commun. ACM*, 64(3): 107–115, 2021. 2
- [73] Zhilu Zhang and Mert R. Sabuncu. Generalized cross entropy loss for training deep neural networks with noisy labels. In *NeurIPS*, pages 8792–8802, 2018. 1
- [74] Yihe Zhou, Tao Ni, Wei-Bin Lee, and Qingchuan Zhao. A survey on backdoor threats in large language models (Ilms): Attacks, defenses, and evaluations. *CoRR*, abs/2502.05224, 2025. 1

# Subtract the Corruption: Training-Data-Free Corrective Machine Unlearning using Task Arithmetic

# Supplementary Material

# A. Training and Hyperparameter Details

#### A.1. Model Details

We use a pre-trained CLIP vision encoder (ViT-B/16) with original OpenAI pre-trained weights. standard practice, we render a number of predefined templates with class names in each dataset, encode them with the CLIP text encoder to build per-class prototypes, average templates per class, and freeze the resulting prototype linear head. The text encoder is then removed from the model, and we fine-tune only the vision encoder. Task vectors are then constructed using the parameters of the vision encoder (excluding the frozen classification Randomly initialized networks use PyTorch's default initialization algorithm, and for pre-trained ResNets and vanilla ViT (ViT-B/16), we use ImageNet1Kv1 Furthermore, for the weights from torchvision. analysis of pre-trained priors with ResNet models, we also use ImageNet1Kv2 weights when available (ResNet50/101), which are slightly more powerful than ImageNet1Kv1. As for DINOv3, we use the version facebook/dinov3-vitb16-pretrain-lvd1689m from HuggingFace.

We note that, when computing task vectors for ResNet models, we exclude all BatchNorm (BN) parameters and buffers (i.e., the affine weights  $(\gamma,\beta)$  and the running mean/variance) and retain their values from  $\theta_{\rm mix}$ . This is because fine-tuning on a fully corrupted proxy dataset induces large shifts in BN running statistics and if these BN deltas are included and later negated from  $\theta_{\rm mix}$ , they overwrite partially calibrated statistics, destabilize activations, and severely degrade performance. Because we cannot reliably recalibrate BN without clean data in our source-free setting, we treat BN as fixed and compute task vectors over the remaining parameters.

#### A.2. CUTS Training Procedure

Across all experiments, we pre-train and fine-tune using the cross-entropy loss and the AdamW optimizer [43, 51] with default hyperparameters, except that we tune the learning rate. Our primary learning rate schedule is cosine annealing with a linear warmup [42]. We extend this schedule with a *hold-steps* hyperparameter that keeps the peak learning rate constant for a fixed number of steps before decay begins; this helps the model fully fit the corrupted samples and prevents premature annealing. For some experiments with ResNets and FC1, we instead use a MultiStep schedule for

fine-tuning. Full training details, including the number of iterations, learning rate, schedule type, and corresponding hyperparameters, are reported in Tab. 12.

For input preprocessing, we use the default transforms provided with CLIP and DINOv3. For FC1, we apply no augmentations and only normalize images using the dataset-specific mean and standard deviation. For ResNets and vanilla ViT, we use RandomCrop with 4 pixels of padding and normalize with dataset-specific statistics when the network is randomly initialized and ImageNet statistics when initialized from ImageNet1Kv1 or ImageNet1Kv2 pre-trained weights.

Additionally, for symmetric label noise experiments, CUTS results are obtained by negating the average of two proxy task vectors,  $\tau_p^1$  and  $\tau_p^2$ , each computed from a proxy dataset  $\mathcal{D}_{\text{proxy}}^i$  with identical input images but independently corrupted labels (different random seeds). This is approximately equivalent to negating each vector separately and then averaging the resulting weights; it leaves the overall conclusions unchanged while providing a slightly lower-variance performance estimate.

For the scaling coefficient estimator  $\hat{\alpha}^*$  in the case of label noise, we calculate the self-agreement score with

$$k = \frac{|\mathcal{D}_{\text{proxy}}|}{2|\mathcal{Y}|}.$$

We observed that the algorithm is robust to the choice of k as long as it is set to be larger than 5 and smaller than  $|\mathcal{D}_{\text{proxy}}|/|\mathcal{Y}|$ . For the coverage rate  $\rho$ , we use  $\rho{=}1$  for all datasets (including Clothing1M) except for CIFAR100 where we use  $\rho{=}0.95$ , as the proxy dataset only contains 10 samples for each class and the corrected model outputted by CUTS, might not predict those specific samples correctly if the samples are hard or boundary instances.

#### A.3. Baselines

Catastrophic forgetting. The hyperparameters used for fine-tuning the Mix model on the  $\mathcal{D}_{proxy}$  dataset without corruption injection are reported in Tab. 12. We fine-tune the models to reach near 100% training accuracy.

**SAP.** For SAP, we use the input images in  $\mathcal{D}_{proxy}$  for projecting the activations. SAP has a hyperparameter  $\alpha$  which the authors state works best when set to 10000. However, we observed that this value would not lead to acceptable results for all noise rates  $\eta$ . Hence, we used the clean version of  $\mathcal{D}_{proxy}$  as a validation set to tune  $\alpha$  and chose

Table 5. Full results for FC1 (for MNIST) and randomly initialized ResNet18 models trained under symmetric (SN) and asymmetric (AN) label noise. Cell values show the utility (UT%). The rightmost column reports the average recovery rate (RR%). Best results are shown in bold; second-best results are underlined.

			MN	NIST+F	C1					CIFAR	10+Re	sNet18					CIFAR	100+R	esNet1	8		Avg.
			SN			A	N			SN			A	.N			SN			A	N	RR
Model	10%	20%	40%	60%	80%	20%	40%	10%	20%	40%	60%	80%	20%	40%	10%	20%	40%	60%	80%	20%	40%	
Mix Oracle	96.5 98.5	92.9 98.4	79.7 98.3	56.2 97.9	26.3 97.1	94.2 98.4	81.9 98.3	83.4 89.7	77.9 88.9	60.0 87.4	38.8 85.0	16.6 79.5	84.2 89.7	74.5 88.7	61.0 68.1	52.6 66.9	38.3 63.9	20.5 57.5	6.7 45.4	56.7 67.6	41.5 63.9	0.0
$Mix- au_r$ SAP CF CUTS	95.6 <b>97.1</b> 96.4 96.5	91.9 <b>96.4</b> 94.9 95.0	79.0 <b>93.8</b> 91.1 93.6	55.5 <b>91.0</b> 87.5 88.4	26.2 69.1 <b>80.1</b> 71.4	94.2 96.9 95.0 <b>97.3</b>	81.9 86.9 90.9 <b>93.6</b>	75.9 83.8 83.6 <b>84.3</b>	66.0 <b>81.2</b> 80.0 <b>81.2</b>	9.9 <u>67.1</u> <b>69.2</b> 65.8	10.1 48.4 <b>57.2</b> 52.7	10.2 19.9 <b>32.0</b> 19.5	79.9 <b>85.4</b> <u>84.1</u> 83.9	57.3 75.0 <b>80.0</b> 79.8	44.2 <b>61.4</b> <u>60.9</u> 60.2	1.2 53.1 <u>53.5</u> <b>54.4</b>	1.0 40.7 41.8 42.1	0.9 <u>24.0</u> <b>26.1</b> 23.3	2.1 <u>8.7</u> <b>11.4</b> 7.9	33.7 <u>57.1</u> 57.0 <b>57.3</b>	1.5 42.0 <b>45.8</b> 44.5	-92.64 <u>26.56</u> 25.84 <b>27.46</b>

the value from the grid  $\mathcal{G} = \{1000, 5000, 10000, 20000, 30000, 40000, 50000, 70000, 100000, 200000, 300000, 400000, 500000, 1000000\}.$ 

**Potion.** Potion only uses one hyperparameter which is the fraction of the dataset used for adaptive percentile calculation. We set this hyperparameter to be 0.01 since the implementation adaptively increases this value until it can bring ASR on  $\mathcal{D}_{proxy}$  below 1%. Furthermore, we set the maximum number of tries to 500, so that the algorithm terminates with the specified condition in all experiments.

# A.4. Reproducibility

All experiments were conducted inside a PyTorch NGC Container with version pytorch:25.05-py3, which provides a fixed and portable software environment. The container includes Python 3.12.3, PyTorch 2.8.0.nv25.05, and the CUDA 12.9 runtime. Experiments were conducted on a single NVIDIA RTX A6000 GPU (48 GB VRAM), while those on the Clothing1M dataset utilized two GPUs. To guarantee deterministic results, a global random seed of 11 was fixed and propagated across all libraries (Python, NumPy, and PyTorch) and devices.

## **B. Extended Results**

#### **Label Corruption**

Table 5 provides a complete overview of the performance of the correction methods on randomly initialized FC1 and ResNet18 models across all noise rates  $\eta$ . It serves as the extended version of Tab. 2.

Furthermore, Tab. 6 summarizes the behavior of the vanilla ViT model under label noise. We also include in Tab. 7 the corresponding evaluation of CUTS on classifiers with a DINOv3 backbone (only at  $\eta$ =40%). Unlike for the CLIP architecture, for which we implemented SAP, the SAP baseline was not implemented for this backbone.

As noted before, CUTS performs particularly well when the initial parameters  $\theta_{\rm init}$  correspond to strong pre-trained weights. Its recovery rate does decrease for randomly initialized networks; however, a similar degradation is observed for all competing baselines. Based on the average recovery rates reported in the rightmost columns of Tabs. 5 to 7, CUTS achieves the highest average performance in every architecture–initialization setting, despite not having access to clean labels.

#### **B.1. Poison Trigger**

The detailed results of applying the correction methods under poison trigger corruption are reported for randomly initialized ResNet18 in Tab. 8, for ViT initialized with ImageNet1Kv1 weights in Tab. 9, and for classifiers with a DINOv3 backbone in Tab. 10. As shown, CUTS outperforms Potion across all architecture–initialization settings. We observed that the Potion algorithm is unstable in the source-free setting and often fails to remove the trigger from the corrupted model using the proxy dataset, even when provided a large trial budget (500 iterations). In some runs, Potion completely fails and severely degrades model utility, resulting in a low average PUS for this baseline, whereas CUTS remains robust across architectures and corruption rates  $\eta$ .

## C. Extended Ablation and Analysis

## C.1. Size of the Proxy Dataset

In order to assess the effect of the proxy dataset size  $(|\mathcal{D}_{\text{proxy}}|)$ , we repeated the CLIP experiments on MNIST, CIFAR10, and CIFAR100 under symmetric label noise at  $\eta \in \{40\%, 60\%\}$ , holding out 10% of the original training split as  $\mathcal{D}_{\text{proxy}}$  (instead of the 2% default used in Tab. 1). Empirically, enlarging  $\mathcal{D}_{\text{proxy}}$  produces a larger weight displacement during proxy fine-tuning and therefore a proxy task vector with a higher  $\ell_2$  norm  $\|\tau_p\|$  (see Tab. 11). Because the estimated corruption vector is  $\hat{\tau}_c = \hat{\alpha}^* \tau_p$ , the estimated scaling coefficient  $\hat{\alpha}^*$  decreases as  $\|\tau_p\|$  grows (the

Table 6. Results for ViT-B/16 model initialized with ImageNet1Kv1 weights trained under symmetric (SN) and asymmetric (AN) label noise. Cell values show the utility (UT%). The rightmost column reports the average recovery rate (RR%). Best results are shown in bold; second-best results are underlined.

			(	CIFAR 1	0					C	IFAR1	00			Avg.
			SN			A	.N			SN			A	.N	RR
Model	10%	20%	40%	60%	80%	20%	40%	10%	20%	40%	60%	80%	20%	40%	
Mix	93.6	90.5	72.7	53.7	21.5	90.6	78.5	78.4	74.2	61.3	42.2	19.1	72.0	52.7	0.0
Oracle	96.1	95.9	93.7	94.2	93.2	95.6	95.4	82.3	82.1	80.0	78.5	73.4	81.5	80.1	100
$Mix - \tau_r$	93.5	90.5	73.5	54.0	21.6	90.6	78.5	78.3	74.2	61.4	42.4	19.1	72.1	52.7	0.22
SAP	93.6	91.9	75.4	64.1	24.3	90.8	78.6	78.0	74.5	63.1	43.7	19.0	72.5	52.6	6.35
CF	93.5	91.6	<u>79.7</u>	<u>75.0</u>	49.1	91.7	87.9	78.7	<u>75.5</u>	66.9	53.6	33.0	74.0	60.6	27.29
CUTS	93.4	91.8	81.6	77.7	<u>41.1</u>	92.8	88.7	78.4	76.0	<u>66.4</u>	52.8	<u>25.4</u>	74.8	62.3	29.12

Table 7. Results for classifiers with DINOv3 backbone trained under symmetric (SN) and asymmetric (AN) label noise at  $\eta$ =40%. Cell values show the utility (UT%). The rightmost column reports the average recovery rate (RR%). Best results are shown in bold; second-best results are underlined.

	MNIST	CIFA	AR10	CIFA	R100	Avg.
Model	SN	SN	AN	SN	AN	RR
Mix	78.5	81.3	83.6	74.0	60.3	0.0
Oracle	99.6	98.8	98.7	91.0	91.0	
$ ext{Mix} -  au_r$ $ ext{CF}$ $ ext{CUTS}$	78.1	80.4	83.2	71.2	60.0	-5.43
	95.8	93.0	94.5	82.4	<u>72.4</u>	61.94
	98.8	<b>95.4</b>	<b>94.6</b>	<b>84.0</b>	<b>78.6</b>	<b>73.52</b>

dependence is monotone but not strictly proportional). For a more controlled comparison of recovery and coefficients in Tab. 11, the ideal protocol would be to fix  $\mathcal{D}_{train}$  and draw both proxy subsets (2% and 10%) from the same 10% holdout. Due to compute constraints, our 2% setting reuses earlier runs where the remaining 98% formed  $\mathcal{D}_{train}$ . This discrepancy should have negligible effects on  $\|\tau_p\|$  (which is dominated by proxy size) but can slightly shift RR and the selected  $\hat{\alpha}^*$ .

# C.2. Cosine Similarity of the Task Vectors

In this section we investigate whether task vector directions carry meaningful information. We compute cosine similarities among the proxy task vector  $\tau_p$ , the random task vector  $\tau_r$ , the joint-training vector  $\tau_{\rm mix}$ , and the vector associated with the catastrophic forgetting baseline,  $\tau_{\rm CF} = \theta_{\rm CF} - \theta_{\rm mix}$ . For symmetric label noise we also report two proxy vectors built from the same proxy dataset input images but with different random labels (obtained using different noise seeds),  $\tau_p^1$  and  $\tau_p^2$ , and their average  $\tau_p^{\rm avg}$  (see Sec. A.2). To compute similarities, we flatten all parameters in each task vector and compute the cosine between the resulting vectors.

The similarity matrices for four experiments with symmetric label noise are shown in Fig. 8. Across all settings,  $\tau_p^1$  and  $\tau_p^2$  have positive cosine similarity, and each

is strongly aligned with their average  $\tau_p^{\rm avg}$ . This indicates that different noise realizations lead to very similar proxy directions in weight space. In particular, the proxy vectors associated with symmetric label noise appear to concentrate around a shared direction that is stable across label noise seeds, consistent with our interpretation of  $\tau_p$  as capturing the (symmetric) label corruption task direction. Moreover, the cosine similarity between  $\tau_p^{\rm avg}$  and  $\tau_{\rm CF}$  is consistently negative (around -0.1), indicating a mild but systematic anti-alignment between proxy fine-tuning and catastrophic forgetting fine-tuning.

Figure 9 reports similarity matrices for asymmetric label noise. In this case, the cosine between  $\tau_p$  and  $\tau_{\rm CF}$  is more strongly negative (down to about -0.45), showing that the proxy direction is more clearly aligned with the negative of the catastrophic forgetting direction than in the symmetric noise case. Together with the quantitative results in Tab. 5, this supports the view that CUTS provides a correction update that is closely related to the clean-label fine-tuning used by the CF baseline. Hence, when only corrupted samples are available (for instance, generated from model mistakes or domain knowledge rules), the proxy based update can act as a viable alternative to CF.

For poison trigger corruption (Fig. 10), the task vectors  $\tau_{\rm CF}$  and  $\tau_p$  are nearly orthogonal in all experiments. This shows that the update induced by proxy fine-tuning points in a direction that is essentially independent of the direction taken by the CF baseline when fine-tuning on clean data. Combined with the empirical observation that the CF baseline fails to reliably remove poison triggers (see Tab. 8), this suggests that, in our setting, gradients from clean samples alone are not sufficient to discover the trigger removal direction identified by the proxy task.

Another observation is that, for models initialized from strong pre-trained backbones (CLIP and DINOv3), the random direction  $\tau_r$  is almost orthogonal to all other task vectors. This suggests that, in the high-dimensional weight space of these models, only a small set of structured directions substantially alter the model behavior, while per-

Table 8. Results for randomly initialized ResNet18 models trained under poison trigger corruption. Columns show utility (UT%) and attack success rate (ASR%). The rightmost column shows the average poison unlearning score (PUS). Best results (PUS) are in bold; second-best are underlined.

			MN	IST					CIFA	AR10					CIFA	R100			Avg.
		%	10	)%	20	)%	2	%	10	)%	20	)%	2	%	10	)%	20	)%	PUS
Model	UT	ASR	UT	ASR	UT	ASR	UT	ASR	UT	ASR	UT	ASR	UT	ASR	UT	ASR	UT	ASR	
Mix Oracle	99.7 99.7	100 0.0	99.6 99.7	100 0.0	99.7 99.7	100 0.0	90.3 90.2	100 0.0	89.9 89.8	100 0.0	89.2 89.0	100 0.0	69.7 68.8	100 0.0	67.5 68.1	100 0.0	66.6 66.9	100 0.0	0.0 85.76
$Mix- au_r$ CF Potion CUTS	16.4 99.6 <b>99.1</b> 86.1	89.2 100 <b>1.6</b> 1.3	11.3 99.6 46.8 <b>74.0</b>	0.2 100 <u>0.7</u> <b>1.7</b>	12.2 99.5 <u>11.4</u> <b>95.6</b>	8.8 100 <u>0.1</u> <b>2.0</b>	53.3 89.7 <b>85.9</b> 69.2	94.0 100 <b>0.9</b> 0.9	60.4 89.1 <b>84.8</b> 62.2	77.7 100 <b>1.3</b> 1.1	72.1 87.4 <b>77.5</b> 73.1	49.4 100 <b>1.2</b> 0.9	45.8 68.2 <b>67.5</b> 58.8	91.0 100 <b>1.1</b> 1.0	37.7 67.2 <b>65.6</b> 52.8	82.2 100 <b>0.0</b> 0.6	50.6 65.7 <b>64.4</b> 60.1	90.7 100 <b>0.0</b> 1.3	10.33 0.0 <u>66.38</u> <b>69.32</b>

Table 9. Results for ViT-B/16 model initialized with ImageNet1Kv1 weights trained under poison trigger corruption. Columns show utility (UT%) and attack success rate (ASR%). The rightmost column shows the average poison unlearning score (PUS). Best results (PUS) are in bold; second-best are underlined.

			CIF	AR10					CIFA	R100			Avg.
	2	%	10	)%	20	)%	2	%	10	)%	20	)%	PUS
Model	UT	ASR	UT	ASR	UT	ASR	UT	ASR	UT	ASR	UT	ASR	
Mix	95.8	100	95.6	100	95.2	100	82.5	100	81.4	100	80.4	100	0.0
Oracle	95.9	0.0	95.8	0.0	95.7	0.0	82.7	0.0	82.6	0.0	81.8	0.0	89.08
$\overline{\text{Mix}} - \tau_r$	95.9	100	95.6	100	95.2	100	82.4	100	81.4	100	80.4	100	0.0
CF	95.5	100	95.5	100	94.9	100	82.0	100	80.7	100	80.4	100	0.0
Potion	95.3	2.3	18.2	1.0	12.3	83.3	82.0	0.8	79.4	2.4	73.0	0.6	57.41
CUTS	90.8	2.1	77.7	2.2	88.2	2.0	<u>79.5</u>	2.3	73.0	1.3	68.3	1.7	78.04

Table 10. Results for DINOv3 model trained under poison trigger corruption. Columns show utility (UT%) and attack success rate (ASR%). The rightmost column shows the average poison unlearning score (PUS). Best results (PUS) are in bold; second-best are underlined.

			CIF	AR10					CIFA	R100			Avg.
	2	%	10	)%	20	)%	2	%	10	)%	20	)%	PUS
Model	UT	ASR	UT	ASR	UT	ASR	UT	ASR	UT	ASR	UT	ASR	
Mix	98.6	100	98.7	100	98.5	100	89.3	100	89.4	100	89.0	100	0.0
Oracle	98.5	0.0	98.6	0.0	98.4	0.0	89.3	0.0	89.2	0.0	88.7	0.0	93.80
$Mix-\tau_r$	98.6	100	98.6	100	98.5	100	89.2	99.6	89.2	100	88.9	100	0.06
CF	98.4	100	98.5	100	98.4	100	88.6	99.6	88.9	99.9	88.2	100	0.07
Potion	98.4	0.8	27.1	0.9	10.1	0.0	87.1	0.0	80.3	0.3	33.4	0.4	55.83
CUTS	<u>98.1</u>	0.6	98.4	1.9	98.0	1.8	<u>85.8</u>	0.5	85.1	1.4	72.8	1.5	88.55

turbations along a random direction tend to leave performance largely unchanged, consistent with the behavior of the  $\text{Mix}-\tau_r$  baseline reported in our tables. In contrast, for randomly initialized classifiers, moving along random directions has a much stronger effect on performance (cf. Tabs. 5 and 8), indicating that the weight space of such models is less geometrically disentangled.

Finally, we observe that both  $\tau_p$  and  $\tau_{\rm CF}$  are nearly or-

thogonal to  $\tau_{\rm mix}$  in all corruption types. Therefore, both the CUTS correction direction defined by  $-\tau_p$  and the CF fine-tuning direction defined by  $\tau_{\rm CF}$  primarily move the parameters in directions that lie outside the joint-training direction defined by  $\tau_{\rm mix}$ .

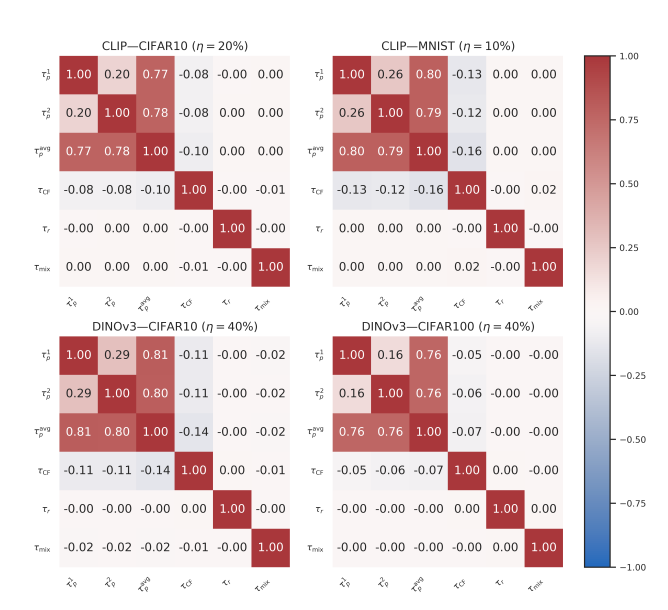


Figure 8. Cosine similarity between task vectors for experiments on symmetric label noise.



Figure 9. Cosine similarity between task vectors for experiments on asymmetric label noise.

Table 11. Comparison between the effect of  $|\mathcal{D}_{proxy}|$  on the norm of  $\tau_p$ , value of  $\hat{\alpha}^*$ , and the recovery rate (RR%) of CUTS, for CLIP models trained on MNIST, CIFAR10, and CIFAR100 under symmetric label noise at  $\eta \in \{40, 60\}$ .

			MN	IST					CIFA	R-10					CIFAI	R-100		
		40%			60%			40%			60%			40%			60%	
$ \mathcal{D}_{proxy} $	$\  au_p\ $	$\hat{\alpha}^*$	RR	$\  au_p\ $	$\hat{\alpha}^*$	RR	$\  au_p\ $	$\hat{lpha}^*$	RR	$\  au_p\ $	$\hat{lpha}^*$	RR	$\  au_p\ $	$\hat{\alpha}^*$	RR	$\  au_p\ $	$\hat{lpha}^*$	RR
2%	0.42	1.5	90.8	0.40	3.0	93.4	0.31	1.4	86.5	0.29	2.0	85.8	0.41	1.35	61.1	0.38	2.0	71.2
10%	1.11	1.4	90	1.06	1.9	91	0.76	1.0	84.9	0.91	1.3	83.6	0.98	0.85	63.32	0.94	1.35	70.1

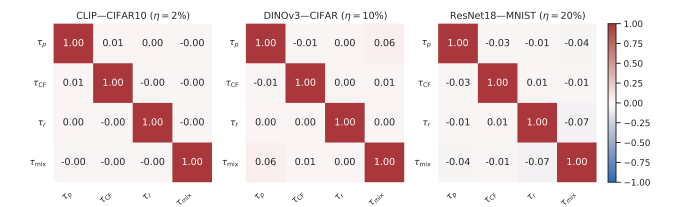


Figure 10. Cosine similarity between task vectors for experiments on poison trigger.

# C.3. Corrected "Clean" Samples for Uncorrupted Training Datasets

We repeated the analysis regarding first flips during correction on models trained on the original (uncorrupted) MNIST and CIFAR100 training sets, without any artificially injected label noise. To construct the corruption task vector, we used samples from the corresponding test sets as proxy datasets. We then recorded the first 64 training examples whose predictions flipped away from their training labels. The resulting sets are shown in Fig. 11 (MNIST) and Fig. 12 (CIFAR100). Qualitatively, many of the samples are likely mislabeled or ambiguous, and the rest are atypical or low-support instances. These results show that even widely used benchmark datasets contain mislabeled or highly ambiguous samples.

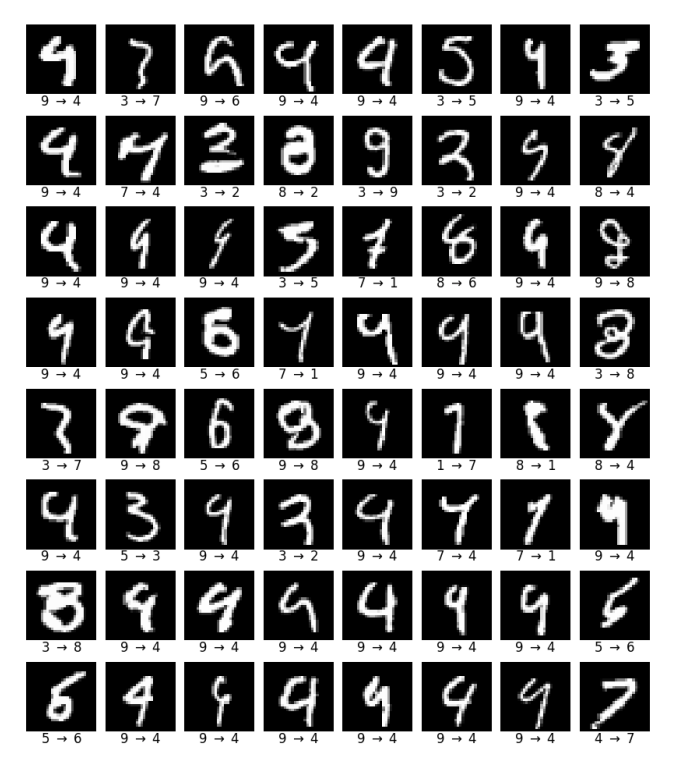


Figure 11. For a CLIP model trained on the uncorrupted MNIST training split, the examples above show the first 64 samples whose predictions flip away from their ground-truth labels when increasing  $\alpha$  along  $-\tau_p$ . The proxy task vector  $\tau_p$  is built using the MNIST test split corrupted with symmetric label noise. Captions show ground-truth  $\rightarrow$  predicted after the flip.

Table 12. Details of the training hyperparameters for different experiments and models. For CLIP and DINOv3, the *Total Iterations* values denote the number of gradient steps, whereas for FC1, ResNet18/34/50/101, and ViT-B/16 they denote the number of epochs. For *Step* schedule, we only specify the number of milestones, and the value of gamma.

			m · ·		1.5	***	TT 11/	D / 1
Experiment		Model	Total Iterations	Max LR	LR Schedule	Warmup/ Milestones	Hold/ Gamma	Batch Size
CLIP SN/AN		Mix	13000	1e-5	Cosine	300	10000	256
	MNICT	Oracle	3000	1e-5	Cosine	300	0	256
	MNIST	Proxy	800	1e-5	Cosine	200	200	256
		CF	500	1e-5	Cosine	100	200	256
	CIFAR10/ CIFAR100	Mix	6000	1e-5	Cosine	300	0	256
		Oracle	3000	1e-5	Cosine	300	0	256
		Proxy	800	1e-5	Cosine	200	200	256
		CF	500	1e-5	Cosine	100	200	256
	MNIST/ CIFAR10/ CIFAR100	Mix	6000	1e-5	Cosine	300	2700	256
		Oracle	3000	1e-5	Cosine	300	700	256
		Proxy	100	1e-5	Cosine	30	20	256
		CF	100	1e-5	Cosine	30	30	256
	Clothing1M	Mix	150000	1e-5	Cosine	1000	79000	256
		Proxy	500	1e-5	Cosine	100	300	256
		CF	500	1e-5	Cosine	100	200	256
DINOv3	MNIST							
		Mix	15000	5e-5	Cosine	300	8000	128
		Oracle	4000	5e-5	Cosine	300	2000	128
		Proxy	600	1e-5	Cosine	100	300	128
		CF	500	1e-5	Cosine	100	200	128
	CIFAR10/ CIFAR100	Mix	12000	5e-5	Cosine	300	8000	128
		Oracle	4000	5e-5	Cosine	300	2000	128
		Proxy	600	1e-5	Cosine	100	300	128
		CF	500	1e-5	Cosine	100	200	128
	CIFAR10/ CIFAR100	Mix	6000	1e-5	Cosine	300	2700	256
		Oracle	4000	1e-5	Cosine	300	1700	256
		Proxy	100	1e-5	Cosine	30	20	256
		CF	100	1e-5	Cosine	30	30	256
FC1 SN/AN	MNIST	Mix	200	5e-4	Cosine	0	0	1024
		Oracle	200	5e-4	Cosine	0	0	1024
		Proxy	300	1e-4	Step	5	0.8	1024
		CF	30	5e-5	Step	5	0.8	1024
ResNet18/34/50/101 PT SNAN	CIFAR-10/ CIFAR-100 RND Init	Mix	150	1e-3	Cosine	0	0	256
		Oracle	150	1e-3	Cosine	0	0	256
		Proxy	120	5e-4	Step	6	0.7	256
		CF	80	5e-5	Step	4	0.9	256
		Mix	120	5e-4	Cosine	0	0	256
	CIFAR10/ CIFAR100 Pretrained	Oracle	120	5e-4	Cosine	0	0	256
		Proxy	120	5e-4	Step	6	0.7	256
		CF	80	5e-5	Step	4	0.9	256
	MNIST/ CIFAR10/ CIFAR100	Mix	120	1e-3	Cosine	0	0	256
		Oracle	120	1e-3	Cosine	0	0	256
		Proxy	200	1e-4	Cosine	30	120	256
		CF	30	5e-5	Cosine	10	10	256
ViT-B/16	CIFAR10/ CIFAR100	Mix	100	5e-4	Cosine	10	50	256
		Oracle	70	5e-4	Cosine	10	30	256
		Proxy	60	1e-4	Cosine	10	20	256
		CF	60	1e-4 1e-4	Cosine	10	20	256
	MNIST/ CIFAR10/ CIFAR100	Mix Oracle	80 60	5e-4 5e-4	Cosine Cosine	10 10	30 20	256 256
			60		Cosine	10	20	256
		Proxy		1e-4				
		CF	60	1e-4	Cosine	10	20	256

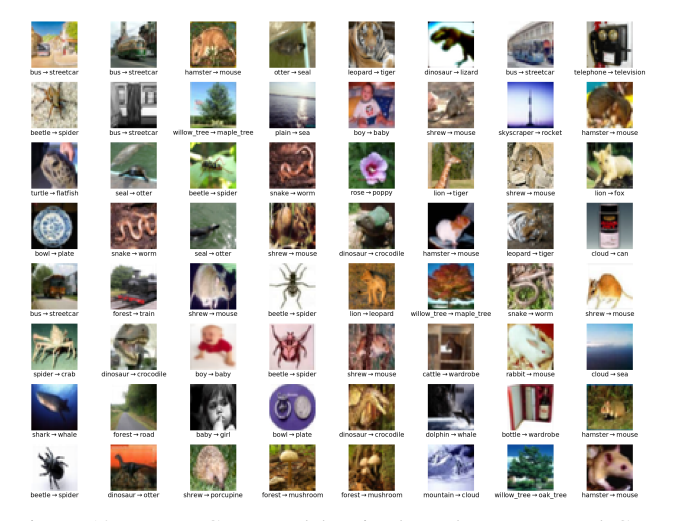


Figure 12. For a CLIP model trained on the uncorrupted CIFAR100 training split, the examples above show the first 64 samples whose predictions flip away from their ground-truth labels when increasing  $\alpha$  along  $-\tau_p$ . The proxy task vector  $\tau_p$  is built using the CIFAR100 test split corrupted with symmetric label noise. Captions show  $ground-truth \rightarrow predicted$  after the flip.